GANIL

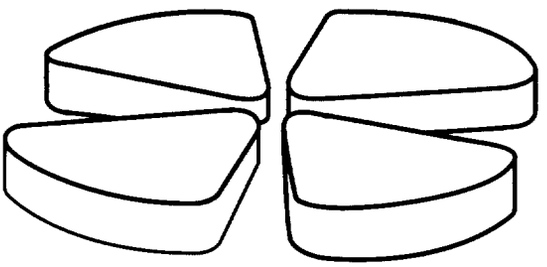

Proton Elastic Scattering on Light Neutron-Rich Nuclei

M.D. Cortina-Gil[1a], P. Roussel-Chomaz[1], N. Alamanos[2], J. Barrette[3], W. Mittig[1], F.S. Dietrich[4], F. Auger[2], Y. Blumenfeld[5], J.M. Casandjian[1b], M. Chartier[1c], V. Fekou-Youmbi[2], B. Fernandez[2], N. Frascaria[5], A. Gillibert[2], H. Laurent[5], A. Lépine-Szily[1,6], N.A. Orr[7], J.A Scarpaci[5], J.L. Sida[2], and T. Suomijärvi[5]

Submitted for publication in Physics Letters B

GANIL P 96 37

Proton Elastic Scattering on Light Neutron-Rich Nuclei

M.D. Cortina-Gil[1a], P. Roussel-Chomaz[1], N. Alamanos[2], J. Barrette[3], W. Mittig[1], F.S. Dietrich[4], F. Auger[2], Y. Blumenfeld[5], J.M. Casandjian[1b], M. Chartier[1c], V. Fekou-Youmbi[2], B. Fernandez[2], N. Frascaria[5], A. Gillibert[2], H. Laurent[5], A. Lépine-Szily[1,6], N.A. Orr[7], J.A Scarpaci[5], J.L. Sida[2], and T. Suomijärvi[5]

1) GANIL (DSM/CEA,IN2P3/CNRS), BP 5027, 14021 Caen Cedex, France
2) CEA/DSM/DAPNIA/SPhN Saclay, 91191 Gif-sur-Yvette Cedex, France
3) Foster Radiation Lab. Mc Gill University, Montreal, Canada H3A 2B1
4) Lawrence Livermore National Laboratory, Livermore, California 94550
5) IPN, IN2P3/CNRS, 91406 Orsay Cedex, France
6) IFUSP, DFN, C.P. 66318, 05315-970, Sao Paulo, S.P. Brasil
7) LPC-ISMRA, Blvd du Maréchal Juin, 14050 Caen, France

Abstract

Proton-nucleus elastic scattering angular distributions have been measured for ^{6}He, ^{7}Li, ^{10}Be, ^{11}Be secondary beams. These data, together with other elastic scattering data for proton on unstable nuclei, have been analyzed using phenomenological and microscopic optical model approaches. To reproduce the experimental angular distributions for unstable nuclei, it was necessary to renormalize either the real or imaginary part of the optical potential. This behaviour is ascribed to break-up.

---

[a] Present address: GSI, Postfach 110552, D-64220 Darmstadt, Germany
[b]Present address: Nucl. Phys. Lab.., Univ. of Washington, Seattle, WA 98195, USA
[c]Present address: NSCL, Univ. of Michigan, East Lansing, MI 48824, USA

Proton-nucleus elastic scattering has been studied extensively and both phenomenological and microscopic optical potential models have been developed to describe the experimental results[1-3]. Within these models it was possible to reproduce a large amount of experimental data with a small number of fixed parameters[3-8]. For example Varner et al.[3] have developed a phenomenological optical potential (CH89) which uses standard form factors for the potential, with the depth and geometry determined from experimental data. The potential includes effective central, surface and spin-orbit terms with energy and nuclear asymmetry dependent parameters which were obtained by fitting measured differential cross sections for proton and neutron elastic scattering on nuclei in the mass range A= 40-209 and for energies between E=10 and 65 MeV. Recently this parametrisation was also shown to give reasonable results for light stable nuclei (A<40) [8]. Other more fundamental potentials have been derived from an effective nucleon-nucleon interaction folded with the nuclear density. For example, the complex microscopic optical potential derived from nuclear matter calculations by Jeukenne, Lejeune and Mahaux (JLM), has successfully described nucleon-nucleus scattering without recall to any free parameters. It has been established that the JLM potential can reproduce successfully proton and neutron elastic scattering angular distributions, provided the imaginary potential is adjusted by a normalization factor $\lambda_w \sim 0.8$[4-7].

With the advent of radioactive nuclear beam facilities, these studies have gained renewed interest, since it then becomes possible to study elastic scattering for nuclei lying far from stability. In particular, the weak binding of such nuclei is expected to lead to modifications of the optical potential[9,10]. In this letter we report a measurement of the differential cross sections for proton elastic scattering on ^{6}He and ^{7}Li, ^{10}Be and ^{11}Be. These data, together with previously published proton elastic scattering data on ^{8}He, ^{9}Li and ^{11}Li [8,11] have been analyzed both in terms of the (JLM) microscopic model and of the phenomenological (CH89) optical potential parametrization.

As described in our earlier papers [12,13], the secondary beams were produced by fragmentation of a 75 MeV/nucleon ^{13}C beam on a 1155 mg/cm^2 thick carbon target located between the two superconducting solenoids of the SISSI device[14] at the entrance to the α-shaped beam analysis spectrometer. The proton elastic scattering was studied using the energy loss spectrometer SPEG[15], which was equiped with its standard detection system[12]. The reaction target was a 100 μm thick polypropylene foil, $(CH_2)_3$.

The elastic scattering of the secondary beams was measured on proton and ^{12}C over the range θ_{lab}=0.7-5.0°. The results from scattering on ^{12}C are the subject of an earlier publication[13]. For the elastic measurements, the emittance of the beam was reduced in the SPEG beam line, such that the angular resolution was of the order of 0.3° and was mainly determined by the divergence of the beam on the target. The energy resolution $\Delta E/E$ was better than 10^{-3}. However owing to the strong kinematic effects of the inverse

reactions, the energy resolution of the proton elastic peak increased with angle and reached $3x10^{-3}$ at the largest angles. The peak corresponding to elastic scattering on hydrogen could be easily identified except in the case of ^{11}Be and ^{7}Li where some contribution from inelastic excitation to the first excited state of these nuclei might occur. The normalization needed to obtain absolute cross sections was derived from the composition of the target and the known cross section at small angles for elastic scattering on ^{12}C which was measured simultaneously[13].

The measured proton elastic angular distributions for ^{6}He, ^{7}Li, ^{10}Be and ^{11}Be are shown in Figs. 1, 2 and 4. These figures also include proton elastic scattering on ^{8}He, ^{9}Li and ^{11}Li as measured by Korsheninnikov et al. [11] and Moon et al. [8]. The beam energies, defined by the magnetic rigidity of the alpha spectrometer, are indicated on the figures. All the angular distributions decrease regularly with θ_{cm}. The ^{8}He, ^{9}Li and ^{11}Li angular distributions exhibit, at angles larger than 40°, an inflection not observed for the Be isotopes. The ^{9}Li and ^{11}Li data in contrast to the other systems, also present a weak structure at the very forward angles.

In Fig.1 the data for the light stable nucleus ^{7}Li are compared to the predictions of the JLM potential using the standard normalization (λ_v = 1.0 and λ_w = 0.8) and that of CH89. For both potentials the agreement is excellent. In particular this shows that the CH89 potential gives good results also for very light nuclei close to the stability valley, although its parameters were adjusted in the mass range A=40-209.

In Fig. 2 the experimental results for the other nuclei are compared to the predictions of the JLM potential. The full lines represent the results obtained using the standard normalization factors. For these calculations density distributions calculated within a Hartree Fock model with shell model occupation probabilities[16], have been used. It has been shown that these densities are in good agreement with the empirical density distributions of the halo nuclei studied in the present work not only in the surface region but also far in the tail. However it should be noted that the corresponding proton and neutron root mean square radii are systematically smaller than the measured ones in the case of the halo nuclei ^{6}He, ^{11}Li and ^{11}Be[17]. In general, the calculated angular distributions overpredict the results, particularly for the most neutron-rich nuclei. In the case of ^{11}Li, we have calculated the JLM potential using different density distributions to test the sensitivity of the calculation to this important but unknown ingredient. Fig. 3 presents the angular distributions obtained with the Hartree Fock density distribution[16] (solid curve), with a nuclear density distribution corresponding to the prescription often used for stable nuclei, i.e. ρ_n=N/Zρ_p (dashed line), and with a microscopic density calculated as

$$\rho_{p,n}(r) = \sum_{p,n} |\Phi(r)|^2$$

where $\Phi(r)$ is the eigenfunction for the protons and neutrons confined inside a potential well which depends on the binding energy of the nucleus[18] (dotted line). In the latter case, the result corresponds to a binding energy of around 500 keV and a root mean square radius of 3.2fm for ^{11}Li close to the experimental value 3.12±0.16 fm [17]. It is clear that the dashed line, which corresponds to the density distribution without a halo, lies furtherest away from the data. It was not possible, however, to reproduce the data with any of the densities, without an additional renormalization of the interaction potential.

The dotted and dashed lines in Fig. 2 are the results of calculations where the normalization factor of either the real or the imaginary part of the potential were allowed to vary. The normalization shown corresponds to the best fit obtained based on a chi-square minimization. The results are summarized in Table 1. Due to the limited angular range covered by the experimental angular distributions, we did not try to reproduce the data by simultaneously varying both the real and the imaginary normalization factors of the potential. To best fit the data the resulting normalization factors of the real potential λ_V are consistently smaller than one. At forward angles the calculated angular distributions (dashed lines) are overall in good agreement with the experimental results, with the exception of the first data points of the angular distributions of ^{9}Li and ^{11}Li for which the experimental cross sections are smaller than the theoretical calculations. The dotted lines correspond to calculations in which the normalization factor of the imaginary part of the optical potential (λ_W) was varied to best reproduce the experimental results. The deduced λ_w are significantly larger than 0.8 for the most neutron rich nuclei. From an inspection of the fits, the angular distributions at forward angles are somewhat better reproduced by calculations employing the renormalized imaginary potential. The deduced normalization factors show variations from the values adopted for stable nuclei which do not seem to scale in a simple way with the isospin of the nuclei. However, the limited angular range covered by the existing data does not allow a definitive conclusion to be drawn yet. At backward angles, $\theta_{cm} > 40°$, all the calculations exhibit an inflection in the slope which is not observed for the system ^{11}Be.

A similar analysis of the data is shown in Fig. 4 using the CH89 optical potential parametrization. The normalization factors of the potential that best reproduce the data are also given in Table 1. In all cases, the best fit values of λ_v and λ_w are very similar to those required for the JLM calculations. This is somewhat surprising given that the CH89 parametrization does not implicitly include any density distribution. It would appear, therefore, that the need to renormalize potentials to reproduce the experimental results is not directly related to any radial dependence of the interaction potential arising from a halo distribution. Such an effect was already encountered in heavy-ion elastic scattering involving weakly bound nuclei, such as ^{6}Li or ^{9}Be[9]. It was shown in these cases that a reduction, by a factor of two of the strength of the calculated real folded potential, is required to reproduce the data. This effect could be related to a dynamic polarization

potential generated in the break up process[19]. Such a potential usually has a positive real part resulting in a decrease of the total real potential and a negative imaginary part which increases the total imaginary potential[10]. Indeed no strong channel coupling effects are included in JLM or any other approaches that use calculations in infinite matter and a local density approximation. This is the major limitation of such approaches, along with the neglect of shell effects which are specific to finite nuclei. The break-up potential is related to the microscopic structure of the nucleus and could explain the non regular evolution of the normalization factors as a function of the isospin.

In summary we have measured elastic scattering differential cross sections for proton scattering on ^{6}He, ^{7}Li, ^{10}Be and ^{11}Be. The results, together with other proton plus unstable nucleus elastic scattering data, were analyzed using a standard phenomenological optical potential and within the framework of a microscopic model employing nuclear matter calculations using realistic nucleon-nucleon interactions and a local density approximation. In order to best reproduce the data, the real potential has to be decreased and the imaginary potential increased for all nuclei, except ^{7}Li for which the standard potentials give satisfactory results. The fact that very similar renormalizations are necessary for two different potentials, a phenomenological one and a microscopic one, where the halo is explicitely included, indicates that the trend observed is not model dependent. Such renormalizations would appear to be related to the break-up processes which should be important for loosely bound nuclei.

The authors are indebted to H. Sagawa for providing the density distributions in a tabulated form.

References

[1] J. P. Jeukenne, A. Leujeune, and C. Mahaux, Phys. Rev. C16 (1977) 80.

[2] F. A. Brieva and J. R. Rook, Nucl. Phys. A307 (1978) 493.

[3] R. L. Varner, W. J. Thompson, T.L. McAbee, E. J. Ludwing, and T. B. Clegg, Phys. Rep. 201 (1991) 57.

[4] F. Petrovich et al., Nucl. Phys. A563 (1993) 387.

[5] J. S. Petler, M.S. Islam, R. W. Finlay, and F. S. Dietrich, Phys. Rev. C32 (1985) 673;

[6] S. Mellema, R.W. Finlay, F.S. Dietrich, and F. Petrovich, Phys. Rev. C28 (1983) 2267.

[7] F. S. Dietrich, R.W. Finlay, S. Mellena, G. Randers-Pehrson and F. Petrovich, Phys. Rev. Lett. 51 (1983) 1629.

[8] C. B. Moon et al., Phys. Lett. B297 (1992) 39.

[9] G.R. Satchler and W.G. Love, Phys. Rep. 55 (1979) 184.

[10] K. Yabana et al., Nucl. Phys. A539 (92) 295, M. V. Andres et al., Nucl. Phys. A589(95) 117, and references therein.

[11] A.A. Korsheninnikov et al. Phys. Lett. B316 (1993) 38.

[12] M. D. Cortina-Gil, These de doctorat, Universite de Caen, July 1996, Rapport GANIL T 96-02 (unpublished).

[13] J. S. Al-Khalili et al. Phys. Lett. B378 (1996) 45.

[14] A. Joubert et al., 1991 Particle Accelerator Conference, IEEE Vol 1 (1991)

[15] L. Bianchi et al., Nucl. Instr. Meth. Nucl. Instr. Meth. A276 (1989) 509.

[16] H. Sagawa, Phys. Lett. B286 (1992) 315.

[17] I.Tanihata, Phys.Lett. B206 (1988) 592

[18] K. Bear and P.E. Hodgson, J. Phys. G 4 (1978) 287

[19] S. Hirenzaki et al, Nucl. Phys. A552 (1993) 57

Figure Caption

Fig.1: Elastic scattering distributions for protons on ^{7}Li. The lines are the results of optical model calculations using the JLM (solid line) and CH89 (dashed line) potentials.

Fig.2: Elastic scattering angular distributions for protons on ^{6,8}He, ^{9,11}Li, ^{10,11}Be. The data for ^{6}He, and ^{10,11}Be are from the present work. The data for ^{9,11}Li are from ref.[8] and that for ^{8}He from ref.[11]. The curves are the results of calculations with the JLM potential. The dashed (dotted) lines correspond to calculations where the real (imaginary) part of the potential have been renormalized (Table 1).

Fig. 3: Comparison of the angular distributions calculated for three different density distributions in the case of ^{11}Li (see text).

Fig. 4: Same as Figure 2 but using the CH89 potential.

Table 1: Normalization factors for each potential that provide best fit to the experimental angular distributions.

	JLM		CH89	
	λv (λw=0.8)	λw (λv=1.0)	λv (λw=1.0)	λw (λv=1.0)
^{6}He	0.9	1.9	0.8	1.8
^{8}He	0.7	1.3	0.7	1.3
^{7}Li	1.0	0.8	1.0	1.0
^{9}Li	1.1	0.8	1.0	0.8
^{11}Li	0.8	1.2	0.8	1.2
^{10}Be	0.9	1.0	0.9	1.1
^{11}Be	0.7	1.4	0.7	1.3

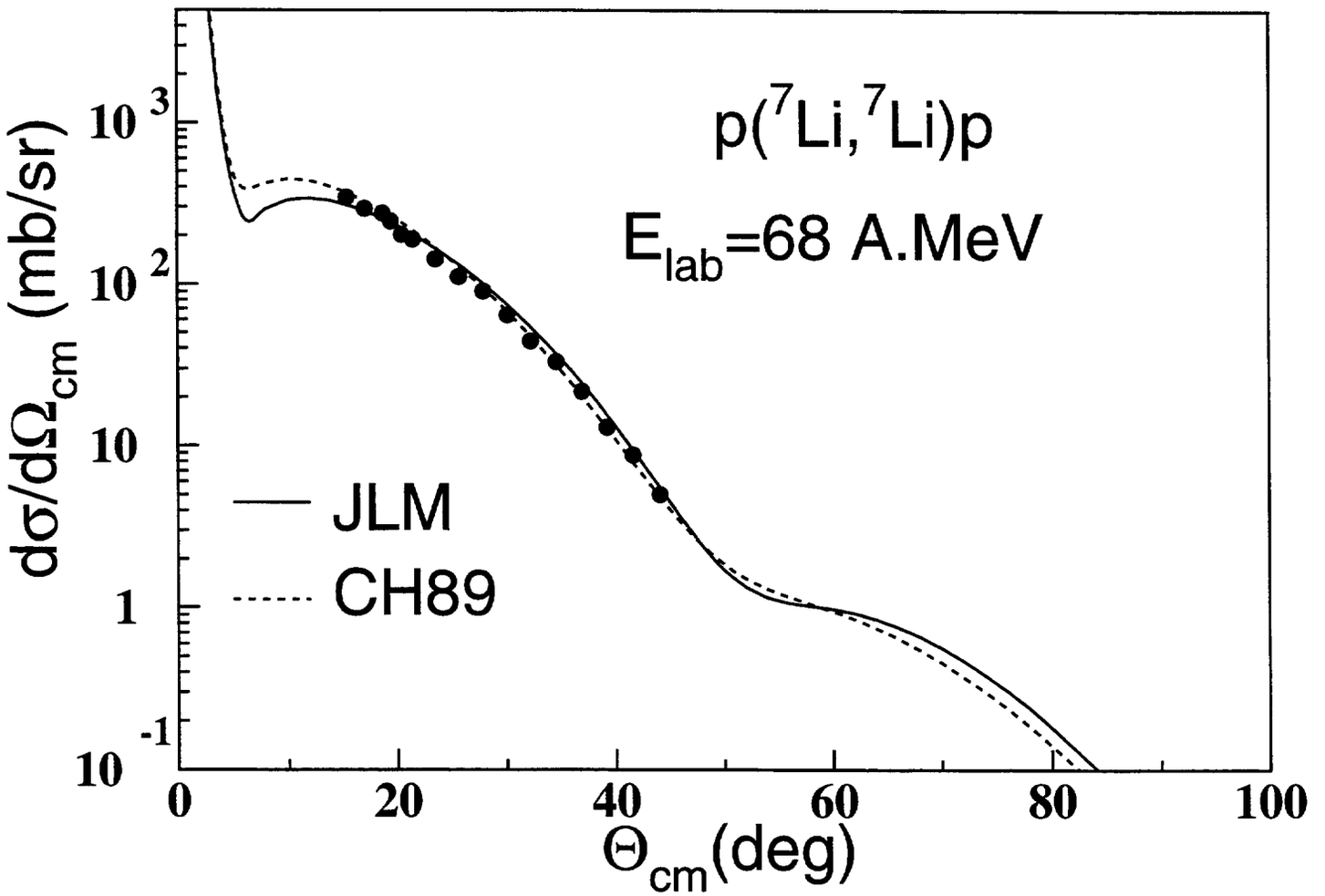
p(7Li,7Li)p
Elab=68 A.MeV
JLM
CH89
dσ/dΩcm (mb/sr)
Θcm(deg)
10 3
10 2
10
1
10 -1
0
20
40
60
80
100

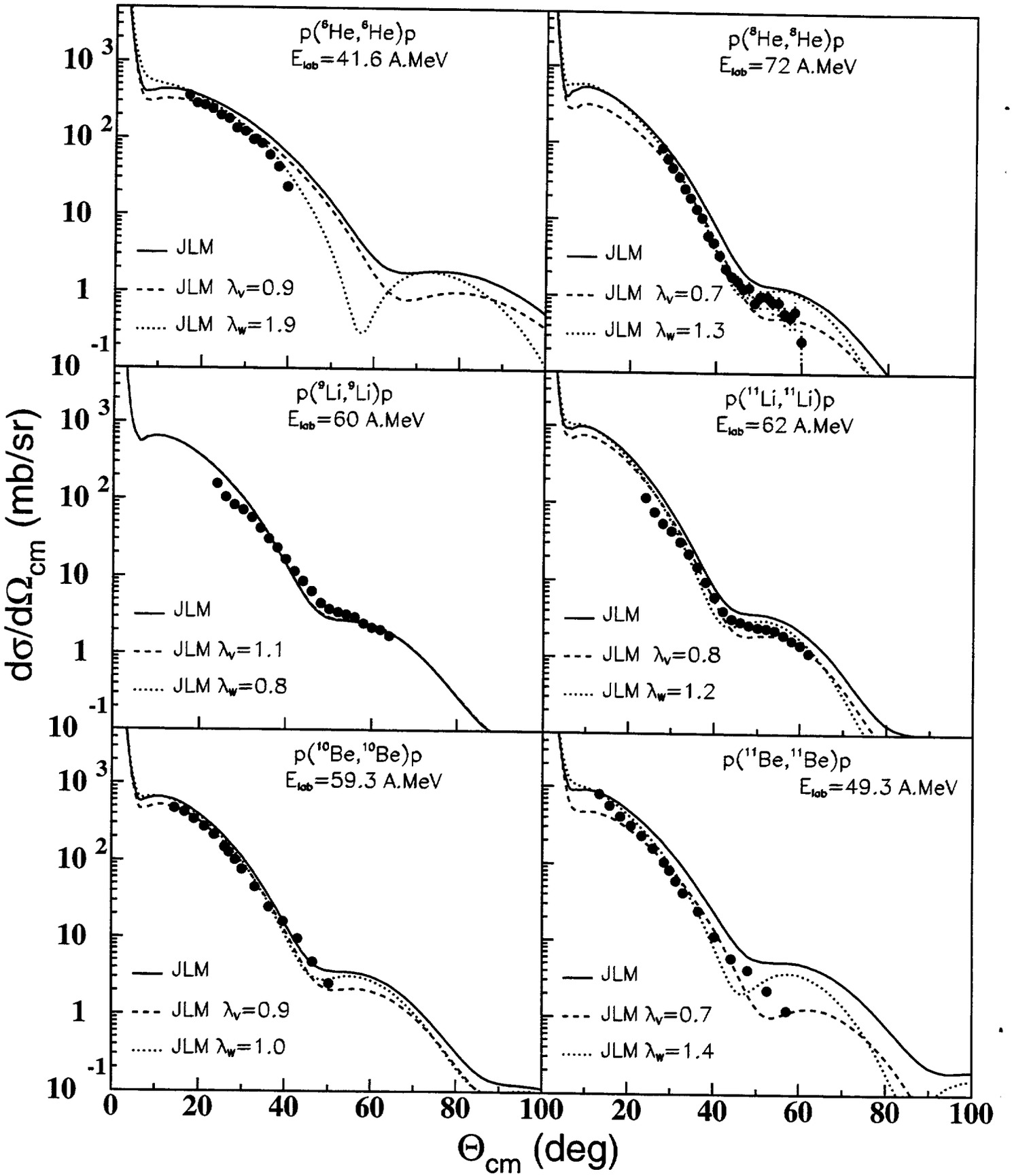
p(⁶He,⁶He)p
E_lab=41.6 A.MeV
JLM
JLM λv=0.9
JLM λw=1.9
p(⁸He,⁸He)p
E_lab=72 A.MeV
JLM
JLM λv=0.7
JLM λw=1.3
p(⁹Li,⁹Li)p
E_lab=60 A.MeV
JLM
JLM λv=1.1
JLM λw=0.8
p(¹¹Li,¹¹Li)p
E_lab=62 A.MeV
JLM
JLM λv=0.8
JLM λw=1.2
p(¹⁰Be,¹⁰Be)p
E_lab=59.3 A.MeV
JLM
JLM λv=0.9
JLM λw=1.0
p(¹¹Be,¹¹Be)p
E_lab=49.3 A.MeV
JLM
JLM λv=0.7
JLM λw=1.4
dσ/dΩcm (mb/sr)
Θcm (deg)

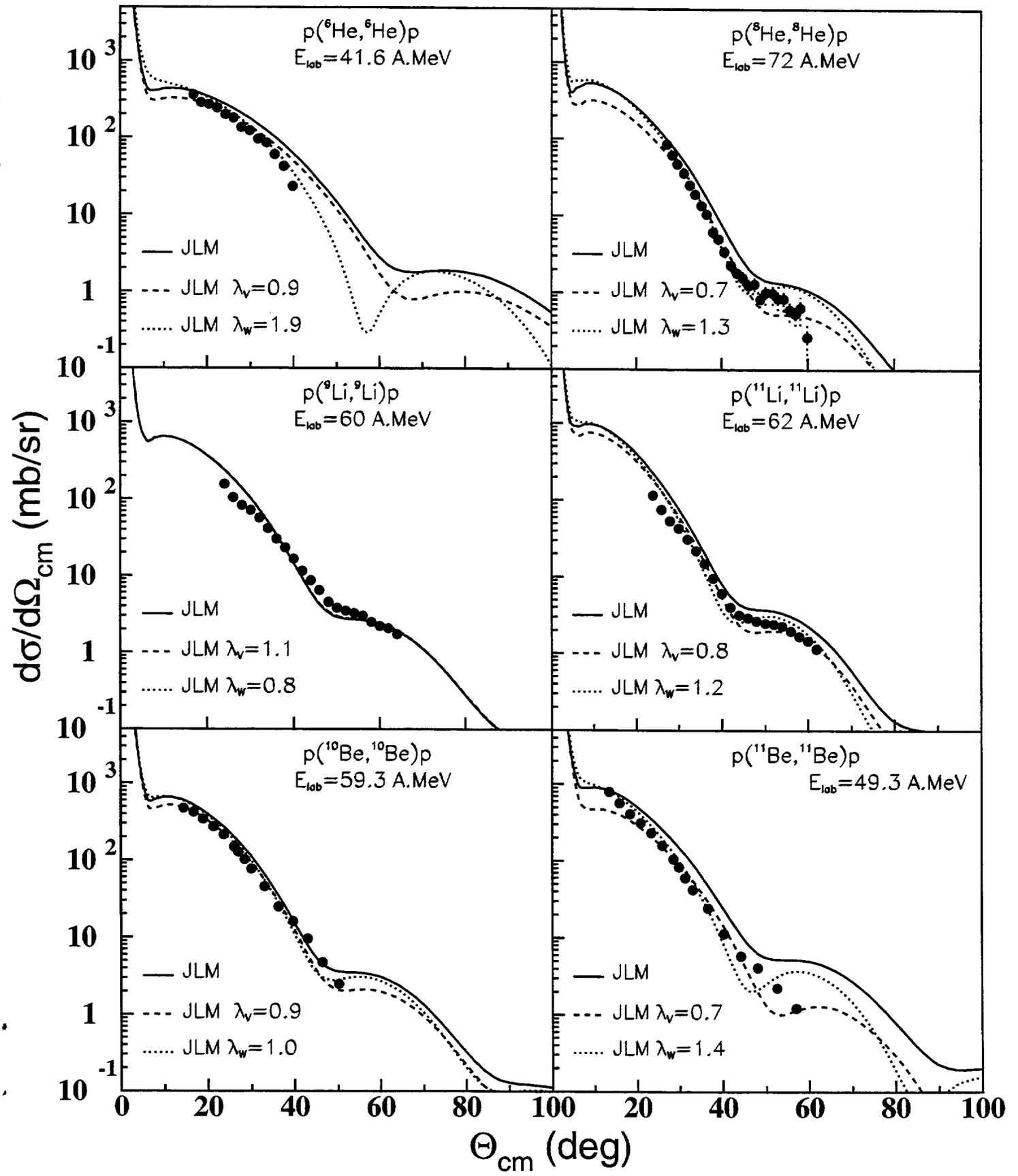
p(⁶He,⁶He)p
E_lab=41.6 A.MeV
JLM
JLM λv=0.9
JLM λw=1.9
p(⁸He,⁸He)p
E_lab=72 A.MeV
JLM
JLM λv=0.7
JLM λw=1.3
p(⁹Li,⁹Li)p
E_lab=60 A.MeV
JLM
JLM λv=1.1
JLM λw=0.8
p(¹¹Li,¹¹Li)p
E_lab=62 A.MeV
JLM
JLM λv=0.8
JLM λw=1.2
p(¹⁰Be,¹⁰Be)p
E_lab=59.3 A.MeV
JLM
JLM λv=0.9
JLM λw=1.0
p(¹¹Be,¹¹Be)p
E_lab=49.3 A.MeV
JLM
JLM λv=0.7
JLM λw=1.4
dσ/dΩcm (mb/sr)
Θcm (deg)

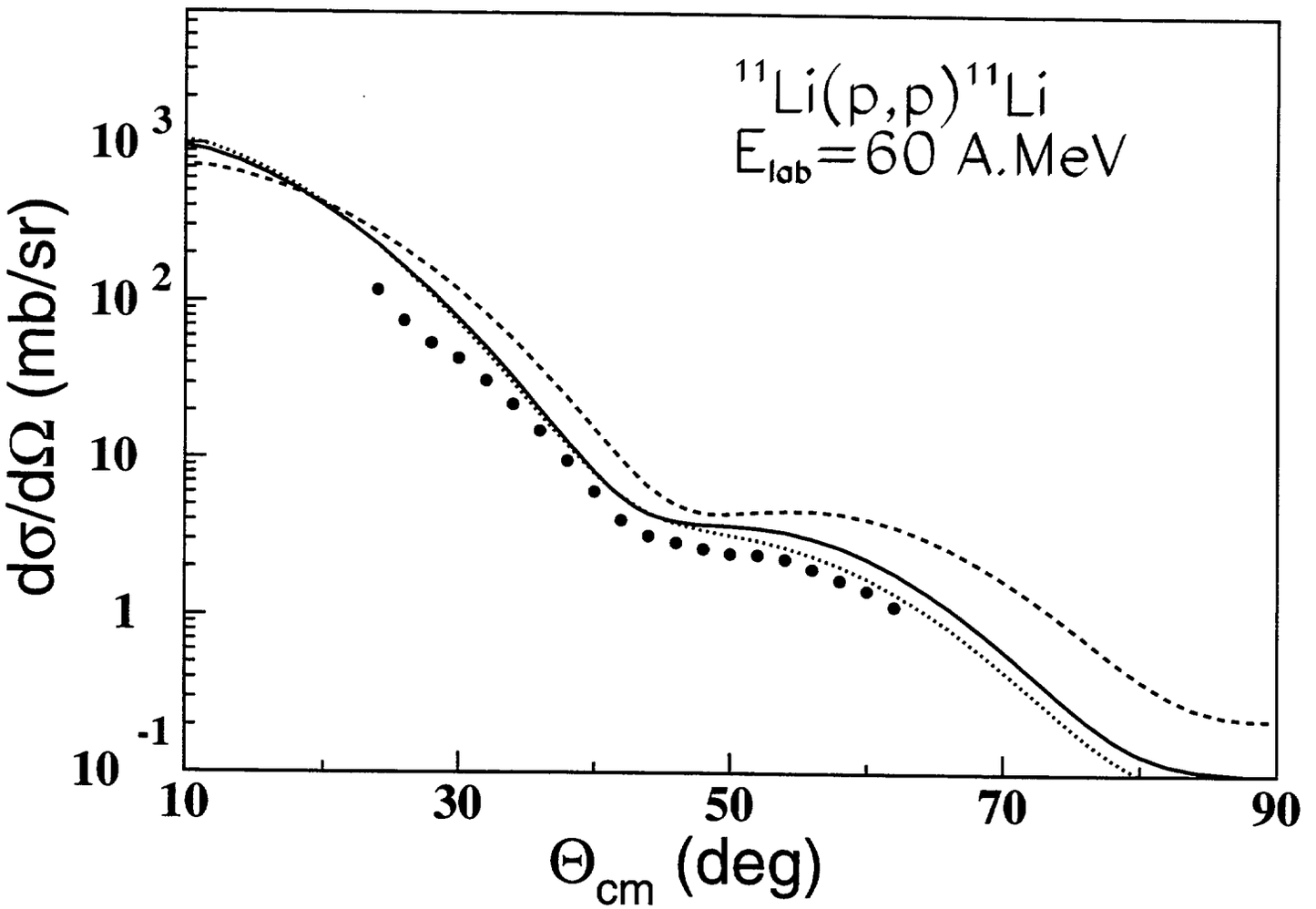
^{11}Li(p,p)^{11}Li
E_{lab}=60 A.MeV
dσ/dΩ (mb/sr)
10^3
10^2
10
1
10^{-1}
10
30
50
70
90
Θ_{cm} (deg)

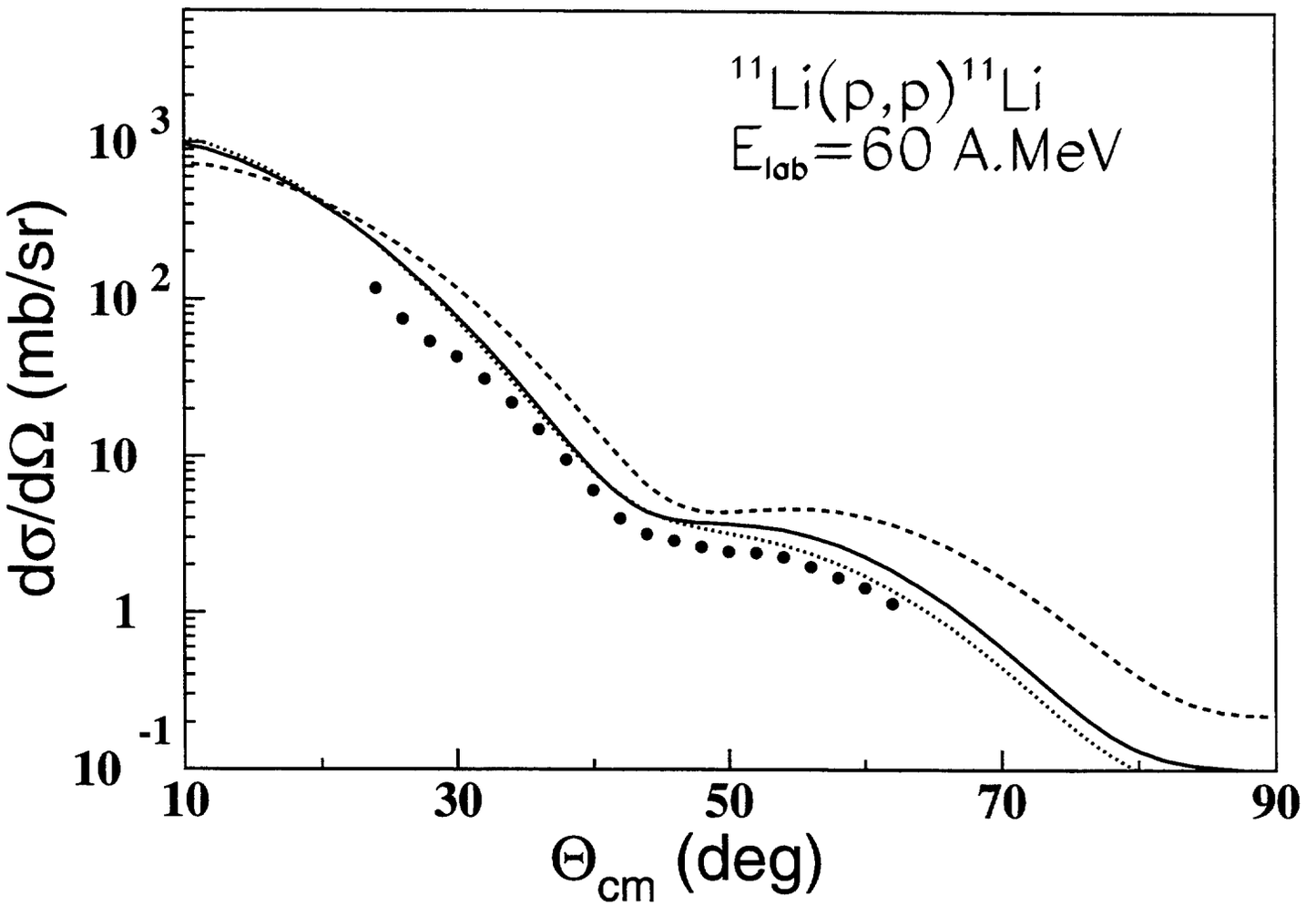
^{11}Li(p,p)^{11}Li
E_{lab}=60 A.MeV
dσ/dΩ (mb/sr)
10^3
10^2
10
1
10^{-1}
10
30
50
70
90
Θ_{cm} (deg)